Clim Dyn
DOI 10.1007/s00382-010-0779-1

Present and future climates of the Greenland ice sheet according to the IPCC AR4 models

Bruno Franco · Xavier Fettweis · Michel Erpicum · Samuel Nicolay

Received: 5 October 2009 / Accepted: 23 February 2010

Abstract The atmosphere–ocean general circulation models (AOGCMs) used for the IPCC 4th Assessment Report (IPCC AR4) are evaluated for the Greenland ice sheet (GrIS) current climate modelling. The most suited AOGCMs for Greenland climate simulation are then selected on the basis of comparison between the 1970–1999 outputs of the Climate of the twentieth Century experiment (20C3M) and reanalyses (ECMWF, NCEP/NCAR). This comparison indicates that the representation quality of surface parameters such as temperature and precipitation are highly correlated to the atmospheric circulation (500 hPa geopotential height) and its interannual variability (North Atlantic oscillation). The outputs of the three most suitable AOGCMs for present-day climate simulation are then used to assess the changes estimated by three IPCC greenhouse gas emissions scenarios (SRES) over the GrIS for the 2070–2099 period. Future atmospheric circulation changes are projected to dampen the zonal flow, enhance the meridional fluxes and therefore provide additional heat and moisture to the GrIS, increasing temperature over the whole ice sheet and precipitation over its northeastern area. We also show that the GrIS surface mass balance anomalies from the SRES A1B scenario amount to -300 km^3/year with respect to the 1970–1999 period, leading to a global sea-level rise of 5 cm by the end of the 21st century. This work can help to select the boundaries conditions for AOGCMs-based downscaled future projections.

Keywords Greenland ice sheet · AOGCMs · Surface mass balance

1 Introduction

Major changes in the Arctic climate have recently been observed (Comiso et al. 2008; Tedesco et al. 2008a; Wouters et al. 2008). Moreover, climate fluctuations influence the global ice volume, and hence sea-level rise (SLR) and ocean circulation (Bond et al. 1993). The Greenland ice sheet (GrIS) is of particular interest because its mass balance variations have an impact on global sea-level fluctuations and oceanic circulation changes. It contributed to sea-level changes more than the Antarctic Ice Sheet during the climatic optimum about 135,000 years ago (Cuffey and Marshall 2000). Zuo and Oerlemans (1997) estimate that the GrIS melting contributed to global SLR with about 3.0 ± 1.6cm between 1865 and 1990. In addition, climate models predict high-latitude amplification of the enhanced greenhouse effect (IPCC 2007). According to the IPCC 4th Assessment Report (IPCC AR4), the contribution of the GrIS melting to global SLR is gauged to 0.21 mm/year for the 1993–2003 period. On the other hand, GrIS mass balance changes are expected to contribute substantially to SLR under the global warming projections for the 21st century (Meehl et al. 2007). Surface warming and the increased freshwater flux induced by a warmer climate could perturb the thermohaline circulation (THC) by reducing the density contrast driving this

Electronic supplementary material The online version of this article (doi:10.1007/s00382-010-0779-1) contains supplementary material, which is available to authorized users.

B. Franco (✉) · X. Fettweis · M. Erpicum
Institute of Geography, University of Liège,
Allée du 6 Août, 2, 4000 Liège, Belgium
e-mail: Bruno.Franco@ulg.ac.be

S. Nicolay
Institute of Mathematics, University of Liège,
Grande Traverse, 12, 4000 Liège, Belgium

Published online: 18 March 2010

circulation (Gregory et al. 2005; Rahmstorf et al. 2005; Swingedouw et al. 2006). In global warming future scenarios, the weakened THC would reduce the heat input to the North Atlantic Ocean and subsequently offset warming in Europe. Finally, the IPCC AR4 estimates that the GrIS is projected to loose mass because increased run-off would exceed precipitation increase. For these reasons, understanding present-day climate in Greenland is essential.

The present research investigates for the current climate (the 1970–1999 period) the set of simulations of the Climate of the twentieth Century experiment (20C3M) performed with atmosphere–ocean general circulation models (AOGCMs) for the IPCC AR4. The aim of this work is to gauge the ability of these models to reproduce the present-day climate conditions over the GrIS. A good representation of this climate is a necessary, but not sufficient condition for the AOGCMs ability to simulate future climate change. A model that fails to reproduce the current climate generates projections (monthly compared to present-day climate outputs) that lack in reliability and validity.

This paper is organized as followed: Sect. 2 details the data and research method. The most suitable AOGCMs for the present-day climate are selected in Sect. 3 by comparing the ECMWF and NCEP/NCAR Reanalyses outputs and observations in situ (ice core measurements and accumulation rates). These models are subsequently used to project climate and surface changes for the last three decades of the 21st century (the 2070–2099 period) in Sect. 4. Section 5 provides estimates of the GrIS surface mass balance (SMB) for the 21st century on the basis of a multiple regression model using anomalies of the current GrIS summer temperature (June–July–August) and annual precipitation.

2 Data description

The data used to investigate the current climate over the GrIS are the set of simulations (run1) performed with AOGCMs (see Table 1) of the IPCC AR4 from the 20C3M. The AOGCMs outputs are monthly-sampled data with a resolution varying from 0.5° to 3.0°, and come from the World Climate Research Programme's (WCRP's) Coupled Model Intercomparison Project phase 3 (CMIP3) multi-model dataset (http://www-pcmdi.llnl.gov/). As in Walsh et al. (2008), these data are linearly interpolated onto a common grid 2.5° × 2.5° (which corresponds to the NCEP/NCAR Reanalysis 1 grid) in order to reduce biases due to the comparison between different spatial resolutions. The AOGCMs results are compared to the ERA–40 Reanalysis from the ECMWF (European Centre for Medium–Range Weather Forecasts) and to the NCEP/NCAR (National Centers for Environmental Prediction–National Center for Atmospheric Research) Reanalysis. Both reanalyses are projected onto the same grid.

Table 1 Models and reanalyses used in this study with their short name and spatial resolution

Data name	Short name	Spatial resolution
BCCR-BCM2.0	BCCR	2.8° × 2.8°
CCCMA-CGCM3.1(T47)	CCCMA-T47	3.7° × 3.7°
CCCMA-CGCM3.1(T63)	CCCMA-T63	2.8° × 2.8°
CNRM-CM3	CNRM	2.8° × 2.8°
CSIRO-Mk3.0	CSIRO-0	1.9° × 1.9°
CSIRO-Mk3.5	CSIRO-5	1.9° × 1.9°
GFDL-CM2.0	GFDL-0	2.6° × 2.0°
GFDL-CM2.1	GFDL-1	2.6° × 2.0°
GISS-AOM	GISS-AOM	4.0° × 3.0°
GISS-EH	GISS-EH	5.0° × 4.0°
GISS-ER	GISS-ER	5.0° × 4.0°
IAP-FGOALS-g1.0	IAP	2.8° × 2.8°
INGV-SXG	INGV	1.1° × 1.1°
INM-CM3.0	INMCM	5.0° × 4.0°
IPSL-CM4	IPSL	3.8° × 2.5°
MIROC3.2 (hires)	MIROC-HR	1.1° × 1.1°
MIROC3.2 (medres)	MIROC-MR	2.8° × 2.8°
ECHAM5/MPI-OM	MPI	1.9° × 1.9°
MRI-CGCM2.3.2	MRI	2.8° × 2.8°
NCAR-CCSM3	CCSM3	1.4° × 1.4°
NCAR-PCM1	PCM1	2.8° × 2.8°
UKMO-HadCM3	HADCM3	3.8° × 2.5°
UKMO-HadGEM1	HADGEM1	1.9° × 1.2°
ECMWF 40 year reanalysis	ERA-40	1.1° × 1.1°
NCEP/NCAR Reanalysis 1	NCEP1	2.5° × 2.5°
NCEP/NCAR Reanlaysis 2 (1979–1999)	NCEP2	1.9° × 1.9°

The AOGCMs short names are based on Leloup et al. (2007). Data source: the World Climate Research Programme's (WCRP's) Coupled Model Intercomparison Project phase 3 (CMIP3) multi–model dataset available at http://www-pcmdi.llnl.gov/. The NCEP2 data are limited to 1979–1999

3 Current climate modelling

As already pointed out by Walsh et al. (2008), the AOGCMs ability to model the general atmospheric circulation and surface conditions (temperature and precipitation) on Greenland must be assessed before making future projections. On this basis, the most suitable global models for Greenland simulation are selected after carrying out a comparison with the reanalyses outputs (ECMWF and NCEP/NCAR) and observations (ice core measurements and/or accumulation rates).

The AOGCMs are assessed over the GrIS by the skill score methodology used by Connolley and Bracegirdle (2007) on Antarctica. The root mean square (RMS) deviation of the multi-annual averaged model field from the multi-annual averaged observed field is calculated. Next this value is normalized by a measure of the variability of this field. This normalized value (RMS_n) is finally rescaled into a weight between 0 and 1, and can be regarded as a measure of the model skill over the GrIS (see Table 2). We refer to Connolley and Bracegirdle (2007) for more details and discussions concerning this methodology.

3.1 General circulation

The AOGCMs atmospheric circulation pattern and its interannual variability over the GrIS are evaluated through the simulated 500 hPa geopotential height.

The main component of the global atmospheric circulation controlling the climatic conditions over the GrIS is the North Atlantic oscillation (NAO), which represents the dominant mode of the regional atmospheric variability around Greenland (Appenzeller et al. 1998; Bromwich et al. 1999; Rogers 1997). The NAO characterizes the large-scale pressure variation between the polar low and the subtropical high (the Icelandic Low and the Azores High, respectively). It is closely related to the Arctic oscillation (AO) (Thompson and Wallace 1998). The NAO index is constructed on a daily basis by projecting the 500 hPa geopotential height anomalies over the northern hemisphere (between Reykjavik and Lisbon). Both the polar low and subtropical high seesaw from year to year (Van Loon and Rogers 1978), defining the NAO phase. As a consequence, the NAO controls the strength and direction of westerly winds across the North Atlantic Ocean, as well as large temperature variations and storm tracks. A positive NAO phase means stronger subtropical high pressure centre and deeper Icelandic Low. This larger difference induces strong winter storms crossing the Atlantic Ocean. It results in warm and wet winters in Europe and eastern Greenland (related to enhanced North Atlantic westerly winds), and cold and dry winters in western Greenland (related to a strengthening of the Baffin Bay northerly winds), as shown by Van Loon and Rogers (1978).

The variability of the surface parameters (temperature and precipitation) are partly induced by the NAO phase. Chylek et al. (2004) have shown that the temperature over West Greenland is significantly anti-correlated to the NAO. When the NAO is in a positive phase, Baffin Bay northerly winds are stronger than normal and oppose weaker than normal westerly winds. This westerly flow usually brings oceanic heat and moisture to west Greenland. Hence, a positive NAO phase results in a lesser snow accumulation along the western coast and heavier precipitation along the GrIS eastern slope, as identified by Appenzeller et al. (1998) and Fettweis (2007), and in lower than usual west Greenland temperatures. On the contrary, when the NAO is in a negative phase, the zonal flow becomes the main component of the large-scale atmospheric circulation around Greenland. It enhances the oceanic moisture transport over the GrIS (Mosley-Thompson et al. 2005) and increases temperatures in western areas, while enhanced northerly flow causes cold winters in eastern Greenland and Europe (Van Loon and Rogers 1978).

The main atmospheric circulation pattern around Greenland can be reproduced by the reanalyses through the annual mean 500 hPa geopotential height (Fig. 1) for the 1970–1999 period. These reanalyses agree with both the regional atmospheric pattern and the 500 hPa geopotential height. This atmospheric pattern results in a large-scale oscillation: an eastward general circulation from the North American continent, adopting a north-east direction over Baffin Bay before reaching the western coast of Greenland,

Table 2 Skill scores for three variables (500 hPa geopotential height, annual near-surface temperature and annual precipitation) according to the skill score methodology used by Connolley and Bracegirdle (2007)

Model name	500 hPa geop height	Temperature	Precipitation
BCCR	0.88	0.22	0.79
CCCMA-T47	0.94	0.44	0.83
CCCMA-T63	0.81	0.42	0.89
CNRM	0.85	0.79	0.85
CSIRO-0	0.95	0.55	0.91
CSIRO-5	0.80	0.40	0.93
GFDL-0	0.95	0.55	0.86
GFDL-1	**0.98**	**0.92**	**0.96**
GISS-AOM	0.89	0.26	0.32
GISS-EH	0.52	0.22	0.55
GISS-ER	0.15	0.69	0.70
IAP	0.97	0.05	0.50
INGV	0.70	0.61	0.86
INMCM	0.72	0.33	0.45
IPSL	**0.98**	0.67	0.87
MIROC-HR	0.65	**0.90**	**0.95**
MIROC-MR	0.97	0.70	0.89
MPI	0.64	0.74	0.94
MRI	0.92	0.29	0.87
CCSM3	0.93	0.87	0.89
PCM1	0.86	0.84	0.91
HADCM3	0.90	0.76	0.92
HADGEM1	0.95	0.83	0.88

For each variable, the best two models are marked in bold

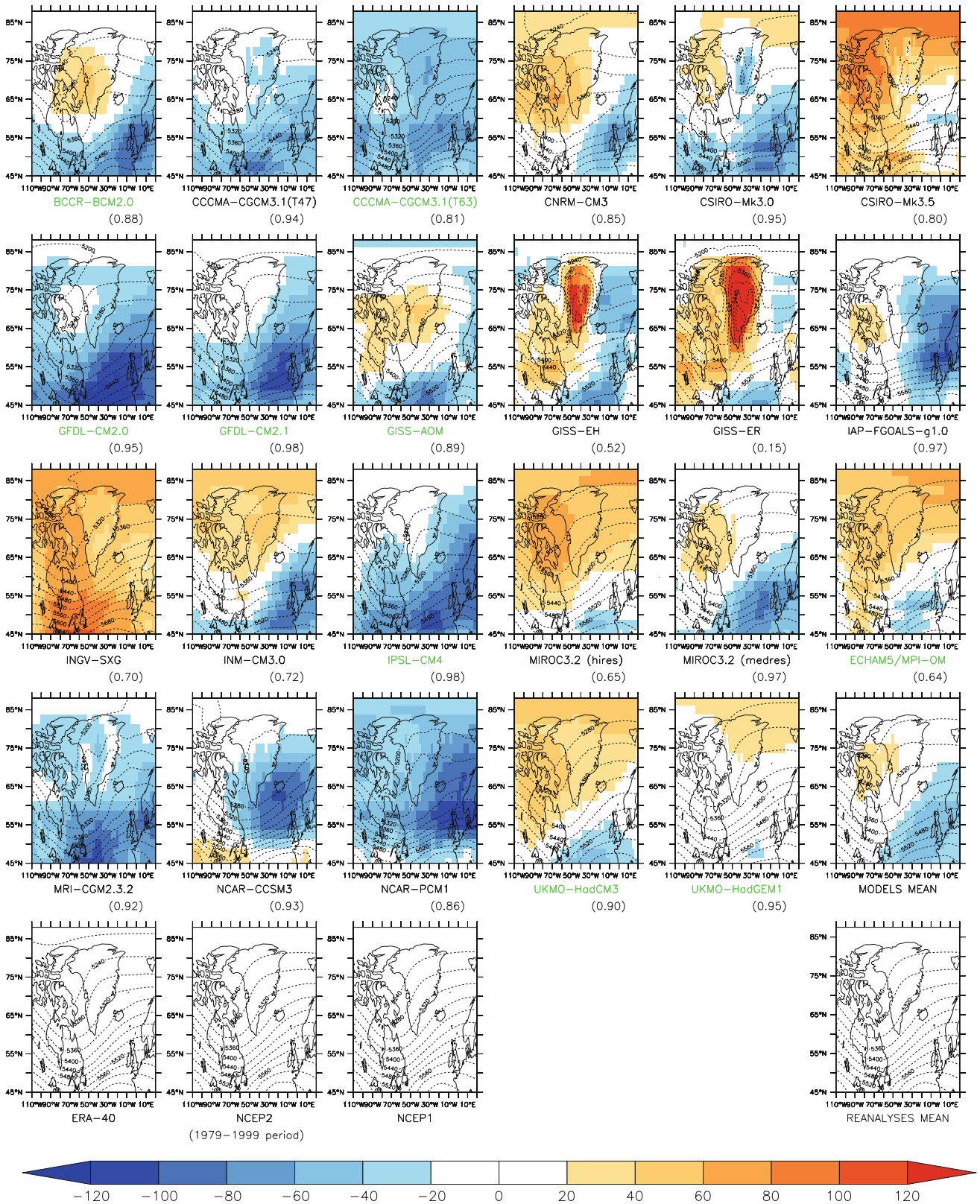

Fig. 1 Difference (in gpm) between the annual mean 500 hPa geopotential height simulated by the AOGCMs (and the AOGCMs average) for the 20C3M experiment and the annual 500 hPa geopotential height from the reanalyses mean (ERA-40 and NCEP1) over 1970–1999. The 500 hPa geopotential height (in gpm) simulated by the AOGCMs is represented with *dashed lines*. The model skill score for this variable is in *brackets*. The names of the efficient AOGCMs for the atmospheric circulation modelling over Greenland are indicated in *green*

and generating an eastward circulation over the central GrIS. In southern Greenland, the regional circulation is more influenced by meridional fluxes. Finally, the 500 hPa geopotential height varies depending on the latitude, from about 5,200 gpm in northwest Greenland to about 5,350 gpm along the southeastern coast.

The 500 hPa geopotential height of the summer months was also investigated; it shows the same pattern over Greenland as the annual mean geopotential height.

The annual mean 500 hPa geopotential height standard deviation (Fig. 2) highlights the areas strongly affected by the interannual atmospheric circulation variability. The reanalyses compare very well and show a high variability area in the southwest of the GrIS (located over the Davis Strait and the southern coast of Greenland). This area is the most affected by the NAO, which enhances or dampens the westerly winds reaching the western GrIS.

In order to test the AOGCMs ability to model the general circulation over Greenland, this study chose to examine the circulation pattern through the annual mean 500 hPa geopotential height (Fig. 1) and its interannual standard deviation (Fig. 2) simulated by the AOGCMs. A correct representation of the 500 hPa pattern, rather than the 500 hPa geopotential height itself, improves the soundness of the general circulation modelling. As discussed previously, the mid-tropospheric circulation (NAO) impacts the surface conditions.

- **Atmospheric circulation pattern**: Nine AOGCMs (BCCR, GFDL-0, GFDL-1, GISS-AOM, INMCM, IPSL, MPI, HADCM3 and HADGEM1) show an atmospheric circulation pattern which is consistent with the reanalyses (Fig. 1). Nevertheless, in other AOGCMs, the circulation comes almost exclusively from the west (CNRM, IAP and MIROC-MR) or keeps a southwest-northeast direction over Baffin Bay and the whole GrIS (CCCMA-T47, CCCMA-T63, INGV and MIROC-HR). Finally, CSIRO-0, CSIRO-5, GISS-EH, GISS-ER, MRI, CCSM3 and PCM1 miscalculate the atmospheric circulation pattern.
- **500 hPa geopotential height**: Most of the AOGCMs which are able to reproduce the atmospheric circulation pattern show 500 hPa geopotential heights close to the reanalyses (Fig. 1). However, it is worth noticing that some models (CSIRO-0, CCCMA-T47, IAP and MIROC-MR) have only a few biases compared to the reanalyses (up to 0.98 as skill score in Table 2), although they model the circulation pattern with some discrepancies.
- **500 hPa geopotential height standard deviation**: Only five AOGCMs (CCCMA-T63, GFDL-0, IPSL, MRI and HADGEM1) are able to simulate the 500 hPa geopotential height standard deviation (Fig. 2) in keeping with the reanalyses. The other global models underestimate the atmospheric circulation variability (NAO).

This last criterion limits the number of efficient AOGCMs for atmospheric circulation modelling over Greenland to only three models: GFDL-0, IPSL and HADGEM1. On the other hand, the MPI and HADCM3 models match quite well with the reanalyses while they underestimate the NAO. Finally, the AOGCMs average has potential to model very well the circulation pattern but totally fails to reproduce the NAO.

3.2 Temperature pattern

In this section, we are comparing the near-surface temperature pattern, its trend, and the near-surface temperature at the top of the ice sheet, simulated by the AOGCMs, with the reanalyses outputs and measurements in situ.

The near-surface temperature is generally the main component of the SMB equation (see Sect. 5 and Fettweis 2007) from which the surface melt can be estimated by using the Positive Degree Day (PDD) approach (Ohmura and Reeh 1991). That is why it is crucial to model it as accurately as possible. The near-surface temperature is directly related to the GrIS topography. Beside the surface temperature, it is influenced by many other parameters such as the dominant regional atmospheric circulation, sea ice concentration in coastal regions, albedo differences between tundra, snow and bare ice surfaces, and volcanic activity. Moreover, Greenland stretches over 2,500 km in latitudinal extent, reaching 770 km south of the Arctic Circle. North-South variations in solar radiation are consequently substantial (Box 2002). In addition, the Greenland topography impedes atmospheric circulation, enhancing northern hemisphere meridional heat exchanges (Barry and Kiladis 1982; Kristjánsson and McInnes 1999).

The GrIS topography is very steep and the complicated orographic features around the margins can only be resolved with a horizontal resolution higher than 25 km, as recently shown by Stendel et al. (2008) in simulation at high spatial resolution with HIRHAM4. This scale is not precise enough to enable a proper representation of all the relevant orographic features of the ablation zone (the latter has a typical width of 100 km). Therefore, near-surface temperature modelling is mainly related to the horizontal resolution of the model: a too coarse horizontal resolution can not efficiently reproduce near-surface temperature in the coastal areas with a complex topography in the ablation zone.

The albedo can also considerably change near-surface temperature. The central GrIS has a high albedo linked to dry snow, and hence reflects efficiently the incoming short–

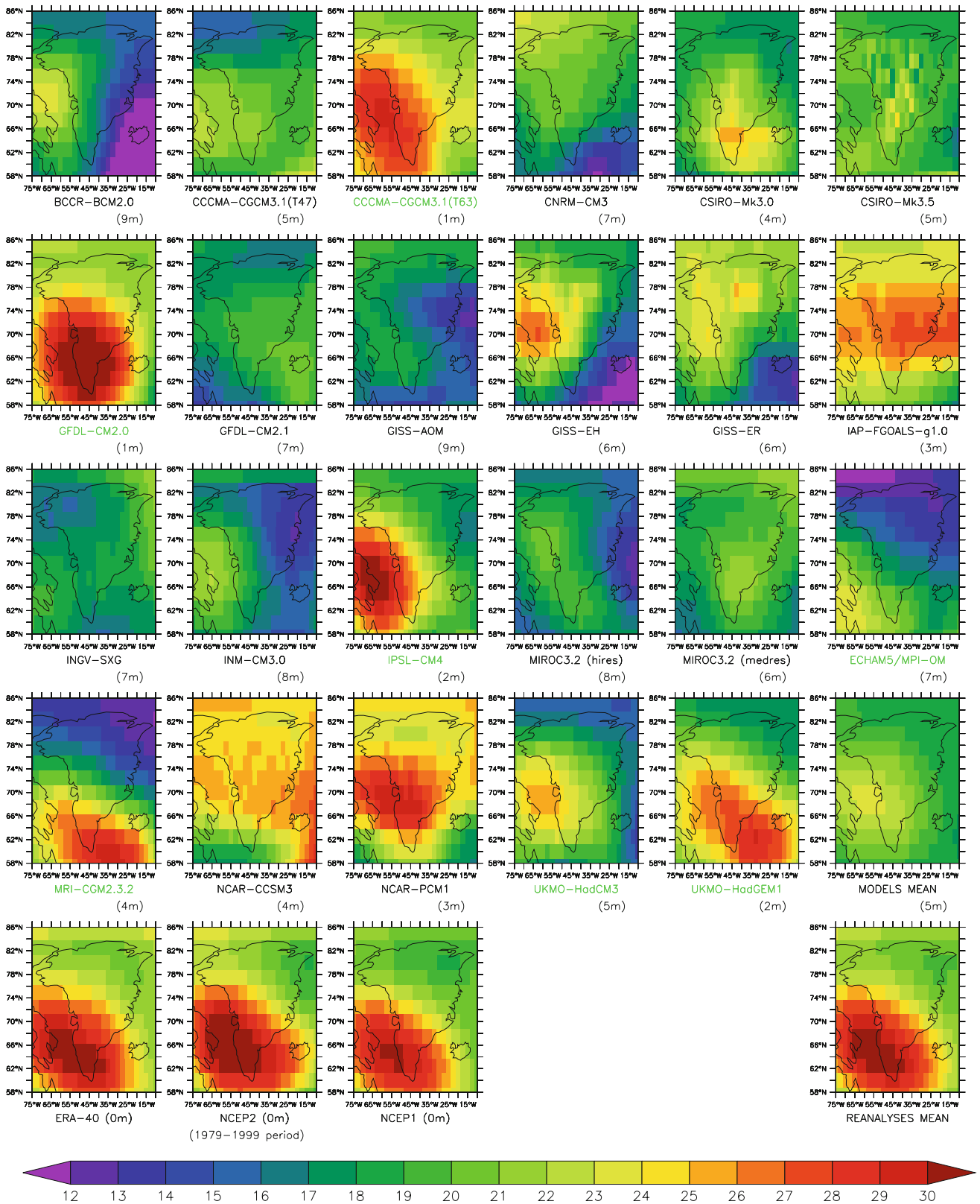

Fig. 2 Standard deviation (in gpm) of the annual 500 hPa geopotential height simulated by the AOGCMs (and the AOGCMs average) for the 20C3M experiment and the reanalyses over 1970–1999. The average of the absolute biases over the GrIS compared to the reanalyses mean is in *brackets*. The most suitable AOGCMs for modelling this variable are indicated in *green*

wave radiation. The main part of the solar radiation is reflected and the quantity of radiation absorbed by the surface is less than the emitted long–wave radiation. This process generates an effective cooling at the surface and a downward transfer of sensible and latent heat from the atmosphere to the surface, leading to a descent of cool air in central Greenland (Dethloff et al. 2002; Gallée and Duynkerke 1997). Because of their typical dissimilarity in reflectance, ice, snow and bare soil change near-surface temperature through albedo feedback in the ablation zone (Fettweis et al. 2005).

It is worth noticing that sea ice plays an important role in coastal temperature variability, because sea ice concentration are invariably larger in the eastern and southeastern areas than in the western and southwestern ones (Cappelen et al. 2001). Coastal sea ice anomalies affect air temperatures, while temperature anomalies affect sea ice thickness and concentration, in a positive feedback loop (Box 2002).

There is a significant anti-correlation between western and eastern Greenland coastal temperature anomalies and the NAO, particularly in autumn and winter (Box 2002; Fettweis 2007; Hurrell 1995; Van Loon and Rogers 1978). Sea ice flux changes in northeast Greenland (Kwok and Rothrock 1999) and sea ice anomalies in the Davis Strait (Parkinson et al. 1999) are also linked to NAO variations.

Over the central GrIS, the annual mean near-surface temperature over the 1970–1999 period is strongly negative (lower than −15°C) (Fig. 3) (due to the altitude and the effective cooling), with a low interannual variability. As pointed out by Box (2002), the largest variations of annual mean temperature are observed along the western coast of Greenland. These parameters can influence considerably near-surface temperature in the ablation zone and coastal regions (Fig. 3), especially in summer. For instance, the annual mean temperature recorded at Nuuk (64.10°N, 51.45°W, 80 m elevation) on the western coast of Greenland is -1.4 ± 2.4°C over the 1961–1990 standard period, and the summer mean temperature is 5.5 ± 1.7°C over the same period. Summer temperature variability in the ablation zone is dampened by the effect of melting snow and ice. As sensible heat affects melting and evaporation, it locks surface temperatures near the melting point (Steffen 1995). Thus, the surface temperature on the ice sheet cannot exceed 0°C because of this process, while surface temperature on the tundra at the GrIS margins is becoming largely positive during summer months.

The 850 and 700 hPa pressure-level temperatures were also investigated; they reveal patterns similar to the near-surface temperature.

In their work to determine the global distribution of temperature changes over 150 years, Jones et al. (1999) indicate opposite temperature trends between western and eastern Greenland. As pointed out by Box (2002), these different trends are mainly induced by the NAO. The 1961–1990 period was characterized by a widespread cooling of about 1.7–2.1°C in central western sites, such as Nuuk (Box 2002). Nevertheless, the NCEP1 and ERA-40 reanalyses do not present particular opposite trends between western and eastern Greenland (Fig. 4) over our 1970–1999 reference period: there is an effective warming (from 2.0 to 5.0°C) in the northern coastal areas and along the eastern coast, while the reanalyses do not show specific temperature trends in western Greenland. Indeed, Box (2002) also observed a statistically significant warming for the 1991–2000 standard decade in the western stations which erases the western negative trends over our reference period (1970–1999). The reanalyses show rather a large north-south contrast: a strong warming (up to 5.0–6.0°C) in northern Greenland but no particular trend over central and southern Greenland (see Fig. 4). The temperature trend pattern of the reanalyses shows the same conclusions over the common 1979–1999 period (electronic supplementary material).

As the NCEP1 data are available from 1948, the near-surface temperature trend is also evaluated over the 1948–1999 period because this longer period can help to reproduce the multi-decadal temperature oscillation over the GrIS. The reanalyses still present a strong warming along the northern and eastern coasts, but also an effective cooling in western and central Greenland. Over the 1958–1999 period (as the ERA-40 data are available from 1958), the temperature trends match quite well with 1948–1999. The corresponding figures are included as electronic supplementary materials.

The temperature at the top of the ice sheet is assumed to be representative for the GrIS temperature variability (Fettweis 2007). According to Box (2002), Steffen and Box (2001) and in situ observations at Summit (72.35°N, 37.38°W, 3208m elevation) obtained from the Danish Meteorological Institute (Cappelen et al. 2001), the annual mean temperature at the top of the ice sheet is ca. −29°C and the summer mean temperature ca. −15°C, over the 1961–1990 standard period.

The mean temperature pattern (Fig. 3), the trends for the 1970–1999 period (Fig. 4) and the mean temperatures at the top of the ice sheet (Table 3) are selected as criteria to investigate the AOGCMs ability for modelling near-surface temperature over Greenland. For this purpose, the AOGCMs and reanalyses annual temperatures are projected onto a common $2.5° \times 2.5°$ grid, but without taking into account the differences between the AOGCM topography and the $2.5° \times 2.5°$ topography. Nevertheless, the temperature of the higher pixel in the model is adjusted to the Summit station altitude with a fixed temperature gradient of −1.0°C/100m (dry air).

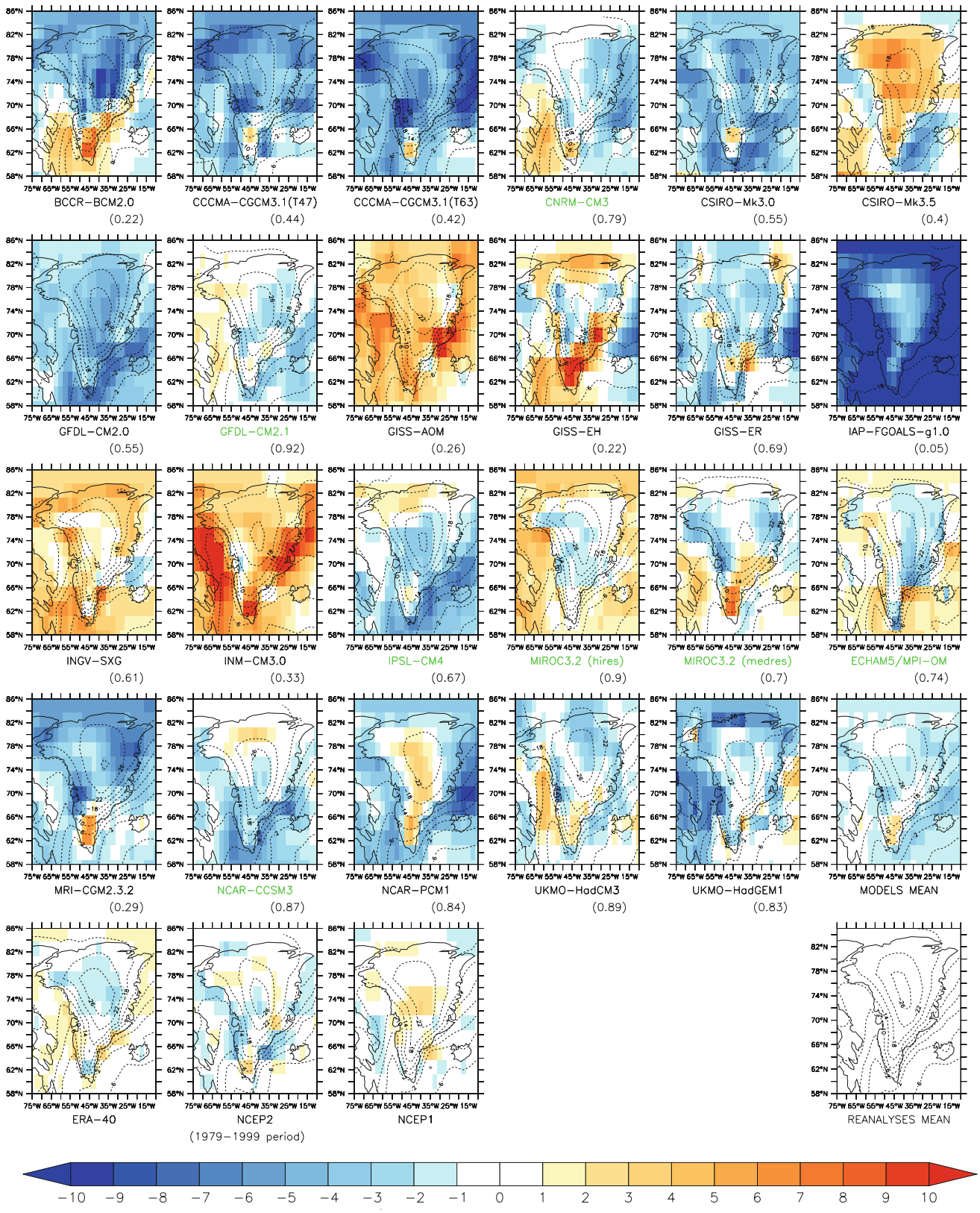

Fig. 3 Same representation as Fig. 1 but for the annual near-surface temperature (in °C)

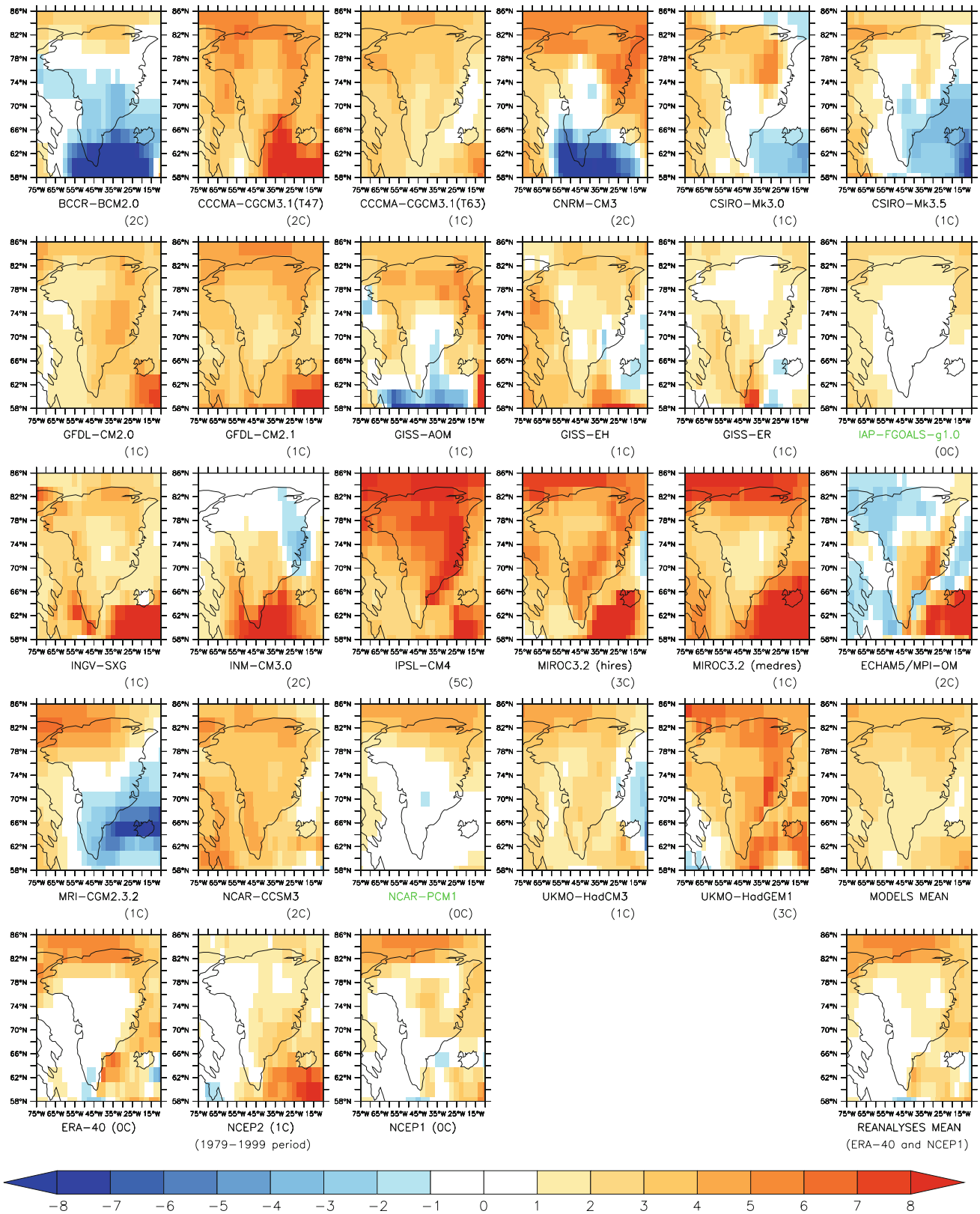

Fig. 4 Same representation as Fig. 2 but for annual near-surface temperature trend (in °C) over the 1970–1999 period

Table 3 Elevation of the highest GrIS pixel (GrIS top), annual precipitation from this pixel (An PP), annual mean temperature (An T°), corrected temperature (An T° corr), summer mean temperature (Sum T°) and corrected summer temperature (Sum T° corr) simulated by the AOGCMs, reanalyses and from observations (Box 2002) at the top of the GrIS

	GrIS top (m)	An PP (mm)	An T° (°C)	An T° corr (°C)	Sum T° (°C)	Sum T° corr (°C)
BCCR	3,121	209.0	−35.45	−36.32	−19.65	−20.52
CCCMA-T47	2,977	143.0	−31.55	−33.86	−17.55	−19.86
CCCMA-T63	3,115	117.6	−33.15	−34.08	−19.15	−20.08
CNRM	3,121	217.1	−27.45	−28.32	−12.65	−13.52
CSIRO-0	3,490	99.9	−30.55	−27.73	−15.75	−12.93
CSIRO-5	3,490	132.4	−20.85	−18.03	−9.75	−6.93
GFDL-0	3,095	103.2	−31.55	−32.68	−17.25	−18.38
GFDL-1	2,986	158.2	−27.65	−29.87	−12.95	−15.17
GISS-AOM	3,089	562.0	−21.55	−22.74	−10.35	−11.54
GISS-EH	3,056	508.0	−26.75	−28.27	−14.75	−16.27
GISS-ER	3,056	508.3	−26.45	−27.97	−15.35	−16.87
IAP	2,408	455.6	−29.75	−37.75	−12.25	−20.25
INGV	3,215	207.9	−26.05	−25.98	−11.65	−11.58
IPSL	2,952	103.8	−29.85	−32.41	−16.55	−19.11
INMCM	2,815	616.9	−22.55	−26.48	−6.75	−10.68
MIROC-HR	3,187	150.0	−27.35	−27.56	−12.35	−12.56
MIROC-MR	2,675	121.7	−26.65	−31.98	−9.05	−14.38
MPI	3,263	87.2	−29.35	−28.80	−18.15	−17.60
MRI	3,146	145.4	−28.15	−28.77	−21.25	−21.87
CCSM3	3,041	221.6	−28.75	−30.42	−14.95	−16.62
PCM1	2,890	172.4	−24.15	−27.33	−8.75	−11.93
HADCM3	3,243	225.1	−27.65	−27.29	−13.75	−13.39
HADGEM1	3,243	126.0	−27.05	−26.69	−14.45	−14.09
ERA-40	3,164	172.3	−27.37	−27.81	−11.53	−11.97
NCEP1	3,319	46.7	−23.91	−22.80	−8.77	−7.66
NCEP2 (1979–1999)	3,319	153.6	−26.85	−25.74	−13.45	−12.34
Summit station (1961–1990)	3,208		−29.10		−14.90	

The simulated mean temperatures are taken over the 1970–1999 period while the observed ones are provided for the 1961–1990 period. The corrected temperature is obtained by adjusting the temperature of the highest pixel to the Summit station altitude (3,208 m elevation) with a fixed gradient of −1.0°C/100m (dry air)

- **Mean temperature pattern**: There are three groups of AOGCMs with regard to the annual near-surface temperature modelling (Fig. 3). In the first one, 13 models (BCCR, CCCMA-T47, CCCMA-T63, CSIRO-0, GFDL-0, GISS-ER, IAP, IPSL, MRI, CCSM3, PCM1, HADCM3 and HADGEM1) simulate far too low temperatures (several degrees discrepancies) compared to reanalyses over the whole GrIS. On the other hand, GISS-AOM, INGV and INMCM simulate much too high temperatures. Finally, the other models show a near-surface temperature pattern in keeping with the reanalyses; among these, GFDL-1 and MIROC-HR have particularly high skill scores (Table 2). However, these AOGCMs still simulate temperature biases (up to 1–2°C) compared to the reanalyses, especially in coastal regions. Part of these discrepancies are very likely due to the differences in topography resolution.
- **Temperature trends**: Only two AOGCMs (IAP and PCM1) are capable of reproducing reliably the near-surface temperature trends over the GrIS (Fig. 4). The other models overestimate temperature trends with high biases (several degrees) compared to the observations, especially in the northern areas (e.g. IPSL or MIROC), or simulate an effective cooling in southern Greenland (e.g. BCCR, CNRM or MRI). In conclusion, the AOGCMs are generally unable to simulate the observed near-surface trends, as already emphasized by Connolley and Bracegirdle (2007) for Antarctica. However, only BCCR, GISS-EH and CCSM3 match quite well with the NCEP1 reanalysis over a longer reference period (1948–1999), while the other models

fail to reproduce the temperature trends over Greenland.

– **Temperatures at the top of the ice sheet (Summit)**: This study assumes hereafter that simulated temperatures for the top of the ice sheet are acceptable if within a range of 3°C to the Summit station measured values. Table 3 shows annual and summer temperatures from ERA-40 and NCEP2 that are quite close to the observed values, but NCEP1 produces biased temperatures. At the top of the GrIS, 12 AOGCMs have annual and summer near-surface temperatures relatively close to the observations (CNRM, CSIRO-0, GFDL-1, GISS-EH, GISS-ER, MIROC-HR, MIROC-MR, MPI, CCSM3, PCM1, HADCM3 and HADGEM1), while most other models underestimate the temperature (e.g. BCCR and IAP). The global models that generally display near-surface temperature pattern in good agreement with the reanalyses fit well with the observations.

Four AOGCMs seem to be able to model near-surface temperature on Greenland (CNRM, GFDL-1, MIROC-HR and CCSM3) although their simulated trends disagree with the reanalyses and observations. The AOGCMs average has potential to model the near-surface temperature pattern around Greenland but is also lacking in modelling the temperature trends.

3.3 Precipitation pattern

The reanalyses outputs, ice core measurements and accumulation rates are hereafter used in order to assess the AOGCMs ability to model the annual precipitation pattern over Greenland and precipitation at the top of the ice sheet.

Precipitation is the main input to the SMB equation (see Sect. 5) by adding snow or liquid water to the ice sheet. The winter accumulation also conditions the aspect of low albedo zones, such as the tundra in summer and the appearance of bare ice in the ablation zone (Fettweis et al. 2005). It has a direct impact on the summer melt intensity, according to Mote (2003) who showed that low ablation years are associated with high winter accumulation. Precipitation needs therefore to be modelled as accurately as possible in order to evaluate the GrIS SMB changes.

Maxima of precipitation and accumulation occur at the southwestern and southeastern coasts of Greenland (Fig. 5) according to ice core measurements (Bales et al. 2009; Kiilsholm et al. 2003) and accumulation rates provided by Burgess et al. (2009, Dethloff et al. 2002). Furthermore, a smaller maximum of precipitation also stretches along the western coast. In these coastal regions, the main precipitation pattern and the strong interannual variability are completely determined by cyclonic activity and the main storm tracks around Greenland (Dethloff et al. 2002). Chen et al. (1997) identified four primary cyclone tracks around Greenland as a result of the thermal and dynamical impacts of the GrIS topography. Around the southeastern coast of Greenland, high precipitation is mainly due to a large-scale humidity transport connected with transient weather systems. Moreover, it is enhanced by substantial orographic lifting near the southern coast (Fettweis et al. 2005). This is the "topographic barrier effect", which modifies the horizontal surface flow or contributes to raise air masses and produce condensation (and thus precipitation during their forced ascent).

There is a minimum of precipitation in the north central part of Greenland (Fig. 5), where annual accumulation is known to be smaller than 200 mm/year (Bales et al. 2009; Burgess et al. 2009; Dethloff et al. 2002). A high pressure area over Greenland drives katabatic winds from the interior plateau towards the Arctic and Atlantic Ocean. The prevailing katabatic winds prevent humidity transports to the northern part of the GrIS (Dethloff et al. 2002).

According to the deep ice core and accumulation rate measurements, Kapsner et al. (1995) found that atmospheric circulation and change in the storm tracks apparently have primary control over snow accumulation in central Greenland. Indeed, the central region of the GrIS acts as a blocking barrier for moving weather systems: it prevents cyclones moving from west to east across the area, and hence, hinders moisture transport (Dethloff et al. 2002). Moreover, effective cooling at the surface and downward heat transfer from the atmosphere to the surface implies air descent over central Greenland. This prevents or reduces cloud cover and promotes the development of surface high pressure. Hence this lack of moisture transports and subsidence over the central GrIS contribute to very low precipitation in this area. At the top of the ice sheet, mean accumulation is near 200 mm/year. The current atmospheric circulation conditions suggest that, near its top, the GrIS is close to a steady state with small accumulation rates. On the contrary, accumulation rates exceed 1400 mm/year at the southeastern coast, and may be significant for coastal glaciers (Bales et al. 2009; Burgess et al. 2009; Dethloff et al. 2002). According to Stendel et al. (2008), the annual precipitation reaches up to 3000 mm/year in this coastal region.

Direct observations of Greenland precipitation are somehow limited. Solid precipitation measurements are mostly collected in coastal regions and mainly confined to locations strongly influenced by orography. In addition, these measurement sites are strongly affected locally by wind, and the induced snowdrift that can be substantial (Dethloff et al. 2002). Therefore, these precipitation measurements are not truly representative of the GrIS

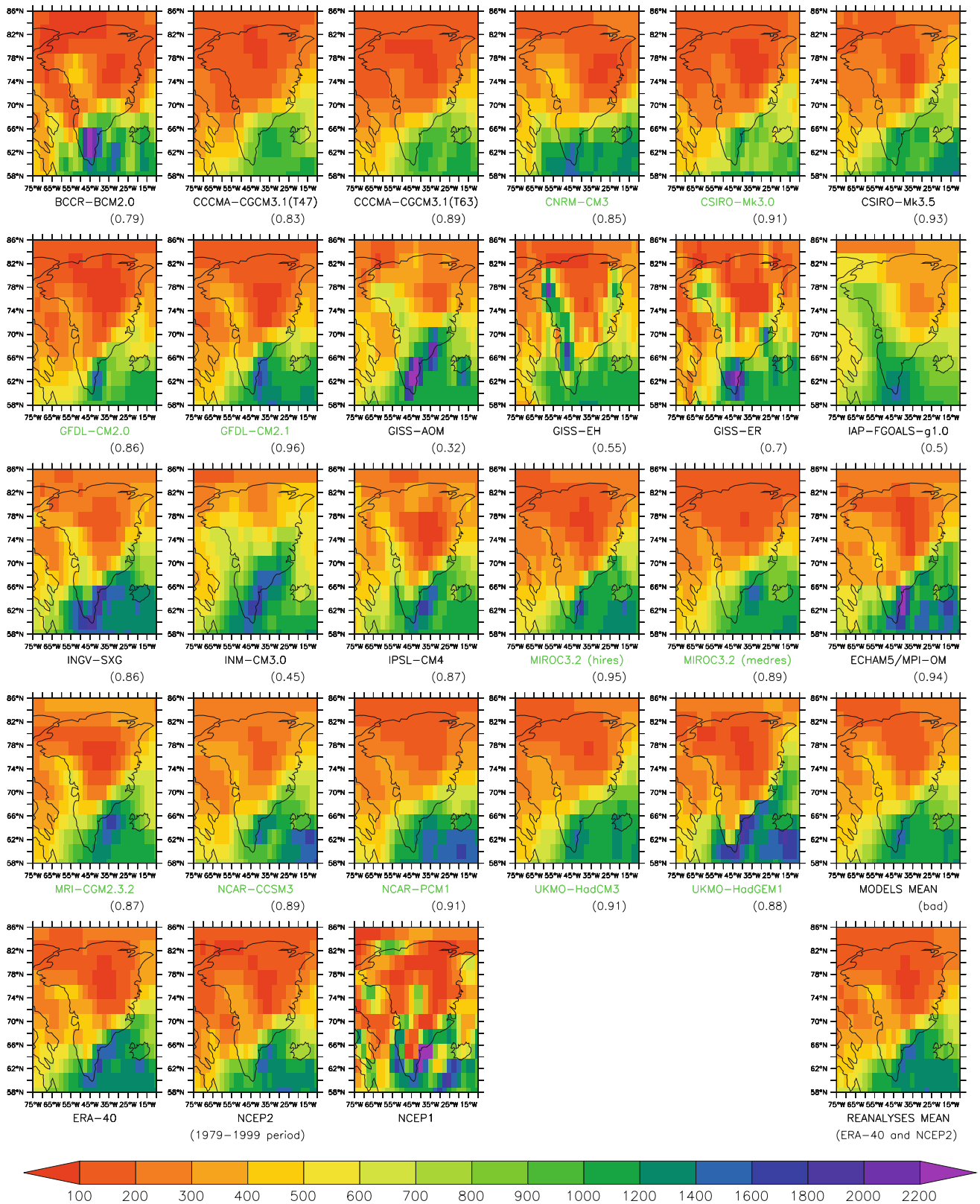

Fig. 5 Annual precipitation (in mmWE/year) simulated by the AOGCMs (and the AOGCMs average) for the 20C3M experiment and the reanalyses over 1970–1999. The skill score for this variable is in *brackets*. The names of the most efficient AOGCMs for the annual precipitation modelling are indicated in *green*

conditions. For these reasons, their use is not sufficient to validate a model established at the scale of the whole GrIS.

Precipitation patterns of the ERA-40 and NCEP2 reanalyses (Fig. 5) are in keeping with the ice core measurements (Kiilsholm et al. 2003) and the accumulation rates provided by Burgess et al. (2009). However, the NCEP1 reanalysis is unable to adequately represent precipitation over Greenland, as already pointed out by Fettweis et al. (2005). The AOGCMs are selected for the GrIS SMB modelling by evaluating precipitation, through the localisation of its maxima and the assessment of precipitation amounts at the north and the top of the GrIS, and by using ice core measurements and reanalyses (ERA-40 and NCEP2). Annual precipitation includes here both solid and liquid precipitation, and is again interpolated onto a common 2.5° × 2.5° grid without topography correction. Since rainfall does not exceed 5% of total annual precipitation over the GrIS, the total precipitation most likely represents fairly well the snowfall.

- **Southeastern maximum of precipitation**: Most global models reproduce the main maximum along the southeastern coast of Greenland (Fig. 5) and are in good agreement with reanalyses, ice core measurements and accumulation rates. Nevertheless, the maximum intensity strongly varies from a model to another: from 1,200 mmWE/year (CCSM3) to more than 2,200 mmWE/year (BCCR). Finally, CCCMA-T47, CCCMA-T63, CSIRO-0, CSIRO-5 and GISS-EH do not simulate any real maximum of precipitation in this coastal region.
- **Lower maximum of precipitation along the western coast**: Only ten AOGCMs (CSIRO-5, GFDL-0, GFDL-1, MIROC-HR, MIROC-MR, MPI, CCSM3, PCM1, HADCM3 and HADGEM1) reproduce the second maximum of precipitation along the western coast of Greenland (Fig. 5). In the other AOGCMs, the western maximum of precipitation is completely absent of the precipitation pattern (CCCMA-T47, CCCMA-T63 and CSIRO-0) or is overestimated (BCCR, CNRM, GISS-EH, GISS-ER, IAP, INGV, INMCM, IPSL and MRI).
- **Precipitation in the north of the GrIS**: Only eleven AOGCMs simulate precipitation amounts lower than 200 mmWE/year along the northern coast of Greenland (BCCR, CCCMA-T47, CCCMA-T63, CNRM, CSIRO-0, GFDL-0, GFDL-1, MIROC-HR, MIROC-MR, MPI and PCM1) (Fig. 5). The other models provide too strong precipitation with a maximum of 500 mmWE/year for this area.
- **Precipitation at the top of the ice sheet**: The BCCR, CNRM, GFDL-1, INGV, MIROC-HR, CCSM3, PCM1 and HADCM3 models have annual precipitation at the top of the GrIS ranging between 150 and 250 mmWE/year (as shown in Table 3) while mean accumulation is near 200 mmWE/year (Burgess et al. 2009; Dethloff et al. 2002). Most of these AOGCMs are able to reproduce the precipitation pattern over Greenland. The annual values provided by the other models vary considerably: from 87 mmWE/year (MPI) to 616 mmWE/year (INMCM).

The criteria were analysed in order to assess the AOGCMs ability to model precipitation over Greenland. The most suitable AOGCMs for these parameters modelling are CNRM, GFDL-1, MIROC-HR, CCSM3, PCM1 and HADCM3 (which have very high skill scores over the GrIS, as shown in Table 2). Nevertheless, in spite of their agreement with the reanalyses, observations and accumulation rates, the MIROC-MR and HADGEM1 precipitation patterns still miscalculate the precipitation amount at the top of the GrIS (Summit). Interestingly enough, a model's huge spatial resolution (lower than 2.5° × 2.5°) is likely responsible for an unsuitable precipitation pattern and/or too heavy precipitation in some regions of the GrIS. Finally, the AOGCMs average makes a conclusive simulation of the GrIS precipitation pattern.

3.4 Selection of the most suitable AOGCMs for current climate modelling

Only few of the AOGCMs investigated here have potential to model the GrIS present-day climate. They are generally capable of reproducing either the general circulation or the surface conditions (precipitation and temperature). Because of these discrepancies, it is difficult to set up a criterion for optimal model selection.

The skill scores can help us in selecting the most efficient models, but this method does not evaluate the accurate modelling of the atmospheric circulation pattern, the location of the minimum/maximum in precipitation, the NAO and the temperature trends.

Hence this study chose a compromise between atmospheric circulation and surface conditions modelling, but emphasizes before all else the AOGCMs ability to reproduce the atmospheric circulation pattern and the NAO. As explained previously, surface parameters (precipitation and temperature) are induced by the regional atmospheric circulation and its dominant variability mode (NAO) around Greenland. In addition, the main goal of this work is to choose AOGCM outputs in order to force later on a regional climate model with atmospheric circulation fully induced by the global model. However, we acknowledge that our model-representation skill approach may be questionable.

Among the AOGCMs capable of reproducing the atmospheric circulation pattern and the NAO, only three

models (MPI, HADCM3 and HADGEM1) simulate the precipitation and temperature patterns in agreement with the observations (as shown in Figs. 1, 2, 3, 4 and 5). Moreover, this selection agree with Walsh et al. (2008) who have already shown that MPI and HADCM3 are top-performing models in simulating the present-day climate (through surface air temperature, precipitation and sea level pressure) over Greenland and Alaska (HADGEM1 was not evaluated in this study).

4 Future projections based on IPCC SRES scenarios

Future projections for Greenland over the 2070–2099 period are performed with the selected global models (the MPI, HADCM3 and HADGEM1 models) and based on the IPCC AR4 outputs of three greenhouse gas (GHG) emissions scenarios from SRES (Special Report on Emissions Scenarios). The B1, A1B and A2 scenarios correspond to a continuous increase of the atmospheric CO_2 concentration for the 21st century up to levels of 550, 720 and 850 ppm by 2100, respectively. The selected AOGCMs outputs are also interpolated onto the common 2.5° × 2.5° grid.

4.1 Atmospheric circulation for the 2070–2099 period

The three selected AOGCMs project over 2070-2099 an atmospheric circulation pattern similar to the one described with the present-day climate simulations, independent of the GHG emissions scenario (Fig. 6a). Nevertheless, the projected positive anomalies of the 500 hPa geopotential are not homogeneous over Greenland. Geopotential height

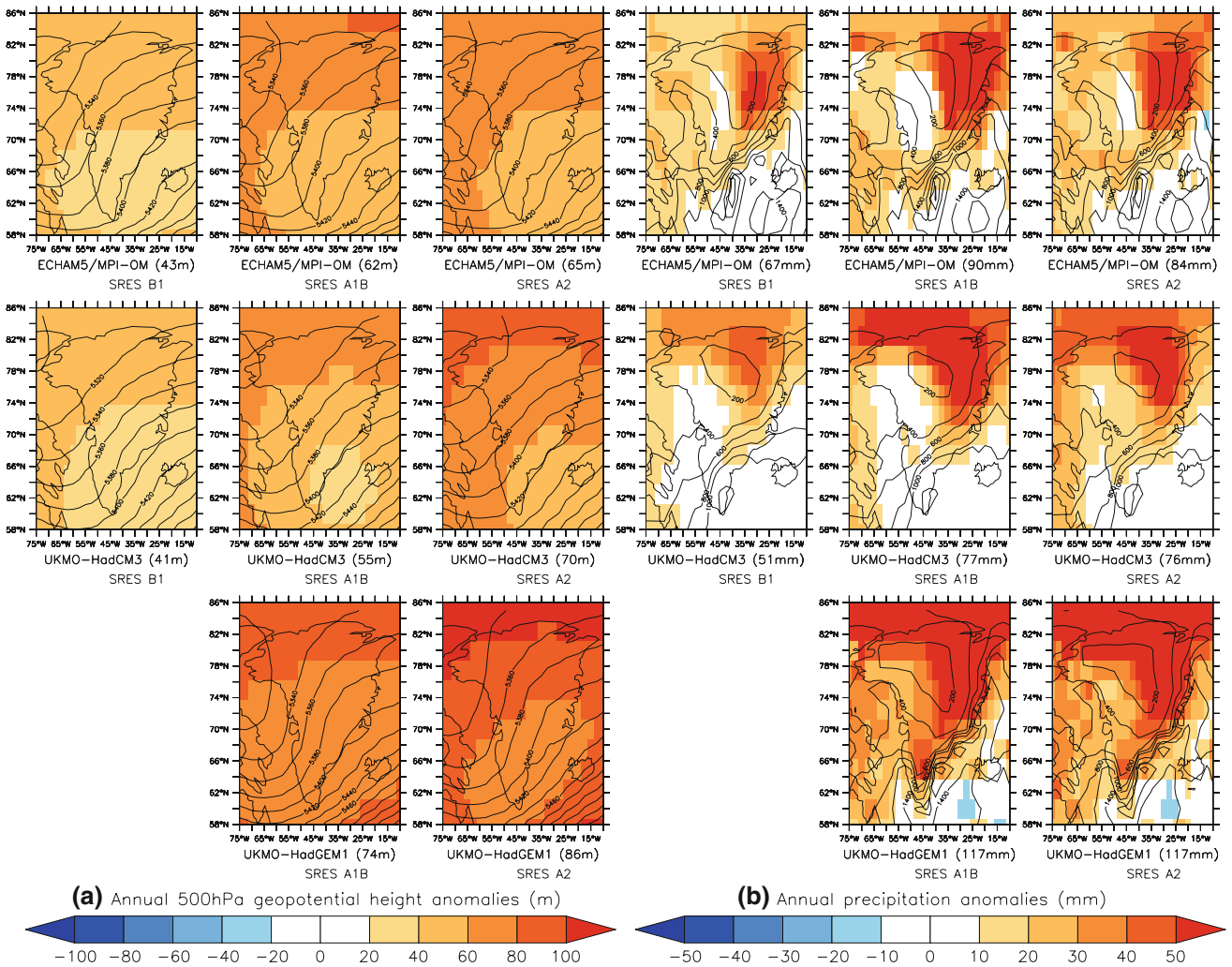

Fig. 6 **a** AOGCMs anomalies (in gpm) of the annual 500 hPa geopotential height for the 2070–2099 period compared to the current-climate 500 hPa geopotential height (from the 20C3M). Projected annual 500 hPa geopotential heights are drawn in *solid lines*. The average of absolute anomalies compared to the 1970–1999 period over the GrIS is in *brackets*. **b** The same as **a**, but for the projected precipitation in mmWE/year. There is no avalaible HADGEM1 results for the SRES B1 scenario on the CMIP3 multi-model dataset website. Compare this figure to Figs. 1 and 5

biases remain low in southern Greenland, but get more pronounced when moving towards the central GrIS and reach their peak along the northern coast, as shown in Fig. 6a. These rises in geopotential height result in strengthening the meridional fluxes. The intensity of these changes is GHG emissions scenario dependant. These anomalies stand at 50 gpm in northern Greenland for the B1 scenario (which projects the lowest increase of the GHG concentration for the 21st century), while they reach 75 and 100 gpm depending on the individual AOGCM for the SRES A2 scenario (which involves the highest GHG concentration rise).

In addition, these geopotential height anomalies involve some local atmospheric circulation changes over the GrIS:

1. a reduction of the east-to-west atmospheric circulation (zonal flow) due to less pronounced projected contrasts between north and south in the 500 hPa geopotential heigh pattern;
2. an enhancement of the meridional fluxes. This intensifies heat and moisture transport from the south to the GrIS, and dampens subsidence in the northern part of Greenland.

4.2 Annual precipitation for the 2070–2099 period

The three selected AOGCMs simulate positives anomalies of annual precipitation almost over the whole GrIS for the 2070–2099 period (Fig. 6b). The annual precipitation projections according to the GHG emissions scenarios point out no substantial change in southern Greenland or along the west coast (from -10 to $+10$ mmWE/year compared to the 1970–1999 period). But the three selected AOGCMs foresee much higher precipitation rises in the northeastern part of Greenland, with values from $+40$ to $+80$ mmWE/year (from $+15$ to $+40\%$ approximately) depending on the GHG emissions scenario.

These future precipitation anomalies can be related to the atmospheric circulation changes over Greenland, as already found out by Krinner and Julien (2007). Indeed, the general westerly circulation produces an onshore moisture flow reaching the western coast of Greenland for the present-day climate, while there is a subsidence (favouring cold air drainage from the top of the GrIS) in eastern Greenland. The central region acts as a blocking barrier for moving weather systems from west to east, preventing moisture transports in eastern GrIS (Dethloff et al. 2002). For the future, the AOGCMs project an increased meridional component of the general circulation bypassing the central region of Greenland and reaching the eastern coast. These circulation changes dampen the subsidence and provide more moisture from the ocean; this process favours precipitation along the eastern coast (Fig. 6b).

4.3 Annual and summer temperatures for the 2070–2099 period

According to the GHG emissions scenarios, the AOGCMs future projections show a significant increase in the annual mean near-surface temperature over the whole GrIS for the end of this century (Fig. 7a). The strongest positive anomalies (up to $+10$°C) occur along the northern coast of Greenland. The warming projected for the northern area is induced by the decrease of sea ice concentration in the closest parts of the Arctic Ocean. A significant warming is also projected along the eastern coast (Fig. 7a). In relation to the northern coast, these temperature rises are related to a reduction in the sea ice concentration (Stendel et al. 2008) and to enhanced meridional fluxes providing more heat to the ice sheet. These temperature anomalies vary from $+4$ to $+8$°C in northern Greenland and along the eastern coast following the increase in GHG concentration foreseen by the IPCC SRES scenarios. Taking into account that HADGEM1 simulates near-surface temperatures over the GrIS that are too low with respect to the present-day climate (as seen in Fig. 3), it is worth noticing that its projected warmings are in this case much stronger than the two other ones, independently of the GHG scenarios. Finally, the central region of Greenland and the top of the ice sheet display lower projected positive anomalies: from $+2$ to $+4$°C.

Summer temperature rises are weaker than the annual changes, and mainly located in the central region of Greenland (Fig. 7b). There is no substantial warming projected along the ice sheet margins, in the ablation zone and in northern Greenland, due to the influence of melting snow and ice. The surface temperature, which highly influences the near-surface temperature, is locked near the melting point (0°C) in summer as long as snow or ice is present. Therefore, the higher anomalies of summer temperatures for the 2070–2099 period are limited to a maximum of $+6$°C compared to the current climate.

4.4 Future projections from non selected AOGCMs

This research has examined the projections over Greenland provided by three other global models (the GFDL-1, MIROC-HR and CCSM3 models). These display a precipitation pattern in accordance with the reanalyses and observations for the 1970–1999 period, but are unable to reproduce the present-day atmospheric circulation. The 500 hPa geopotential height, annual precipitation, and near-surface temperature changes are assessed for the 2070–2099 period according to the AOGCMs outputs (interpolated onto the common $2.5° \times 2.5°$ grid) for the SRES A1B scenario; this scenario was chosen because it is a mid-range GHG emissions scenario.

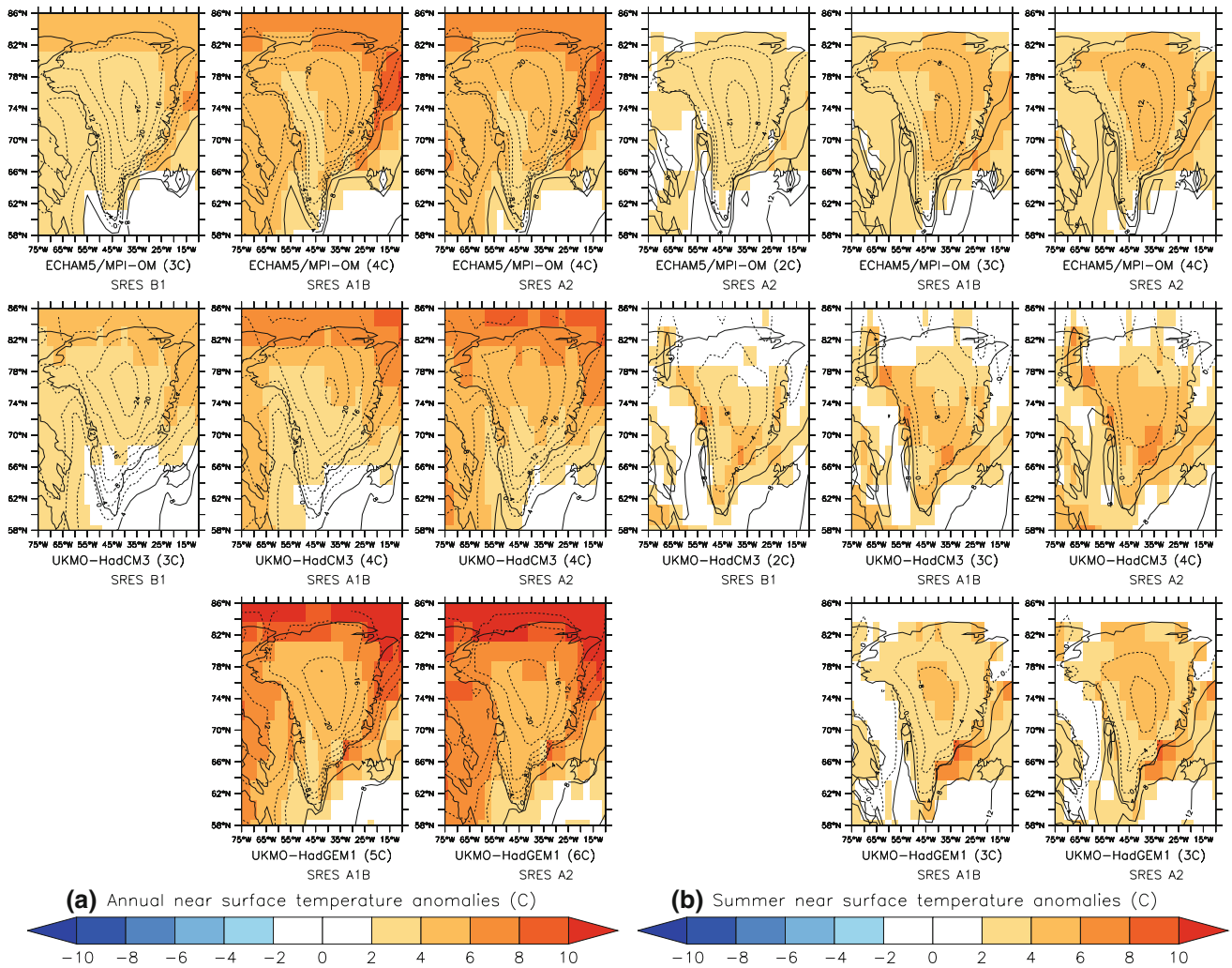

Fig. 7 **a** AOGCMs anomalies (in °C) of the annual near-surface temperatures for the 2070–2099 period compared to AOGCMs annual near-surface temperatures for the 1970–1999 period. Projected near-surface temperatures (in °C) are drawn in *solid lines* (positive temperatures) and in *dashed lines* (negative temperatures). The average of annual near-surface temperature anomalies over the GrIS compared to the 1970–1999 period is in *brackets*. **b** The same as **a**, but for the summer near-surface temperatures (June–July–August). Compare this figure to Fig. 3

Figure 8a shows differences between the atmospheric circulation patterns projected by these global models for the 2070–2099 period and the results of the three selected AOGCMs investigated in the previous section. The GFDL-1 model simulates a strong east-to-west atmospheric circulation over the GrIS, the MIROC-HR model projects very high geopotential heights, and the circulation pattern from the CCSM3 model is rather ambiguous, while the three selected AOGCMs are in perfect agreement.

Although the precipitation anomalies maximum is still located in northeastern Greenland, the future precipitation patterns slightly differ from the ones simulated by the three selected AOGCMs (Fig. 8b). The GFDL-1 simulations calculate lower anomalies (with a maximum of +40 mmWE/year) in this area than the three selected AOGCMs (+80 mmWE/year). The MIROC-HR and CCSM3 models project high annual precipitation changes (from +30 to +40 mmWE/year) along the western and southern coasts of Greenland (i.e. the main melting areas), while the three selected AOGCMs simulate no substantial changes (from −10 to +10 mmWE/year) for the same regions.

Finally, the future annual and summer mean temperatures (Fig. 8c, d) are quite close to those provided by the three selected AOGCMs for the 2070–2099 period (excepting the GFDL-1 model which simulates lower temperature anomalies). Positive anomalies are visible over the whole GrIS and the highest positive anomalies are still located in northern Greenland.

All these comparisons suggest that IPCC global models unsuitable for reproducing a correct atmospheric

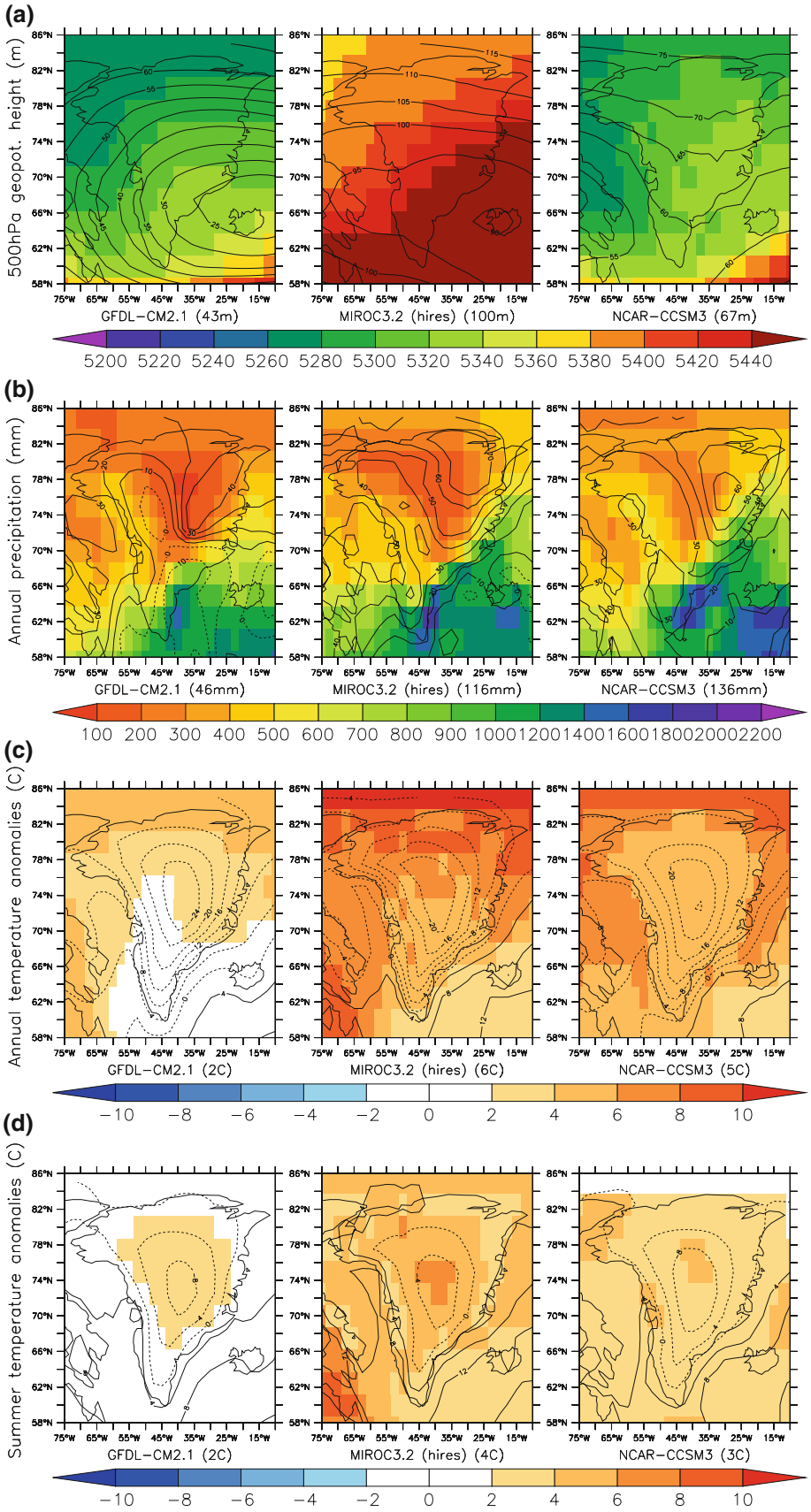

Fig. 8 **a** Annual 500 hPa geopotential height (in gpm) simulated by the GFDL-1, MIROC-HR and CCSM3 models for the A1B scenario over 2070–2099. Anomalies (in gpm) compared to the present-day 500 hPa geopotential height average are drawn in *solid lines* (positive anomalies) and in *dashed lines* (negative anomalies). The average of absolute 500 hPa geopotential height anomalies compared to the 1970–1999 period over the GrIS is in *brackets*. **b** The same as **a**, but for the annual precipitation (in mmWE/year). **c** Future projected anomalies (in °C) of the annual near-surface temperature over 2070–2099. Projected near-surface temperatures (in °C) are drawn in *solid lines* (positive temperatures) and in *dashed lines* (negative temperatures). The average of annual temperature anomalies compared to the 1970–1999 period over the GrIS is in *brackets*. **d** The same as **c**, but for the summer near-surface temperatures (June–July–August)

circulation pattern for the present-day climate project divergent precipitation patterns for the 21st century.

5 GrIS SMB projected anomalies for the 21st century

This section is assessing the GrIS SMB anomalies from 2010 to 2100, based on a multiple regression model set up by Fettweis et al. (2008), and using the selected AOGCMs outputs for three IPCC GHG emissions scenarios. The GrIS SMB variability (ΔSMB_{GrIS}) for the present-day climate can be approximated by the GrIS annual precipitation anomaly ($\Delta P_y r$) minus the GrIS variability rate of melt-water run–off over the GrIS. According to Box et al. (2004) and Fettweis (2007), the total GrIS run-off variability can be parameterized by the mean GrIS summer 2 m-temperature (ΔT_{JJA}) to give this multiple regression:

$$\Delta SMB_{GrIS} \approx a\Delta T_{JJA} + b\Delta P_{yr}$$

where a and b are constant parameters, which are determined for the 1970–1999 period by solving a multiple regression equation, making use of both the JJA temperatures and annual precipitation anomaly time series (computed on specific regions) from the 20C3M experiment and SMB outputs from the regional climate model MAR (Modèle Atmosphérique Régional) from Fettweis (2007) as well as the model from Hanna et al. (2008). Further details and caveats about the multiple regression model and the parameters it used are given in Fettweis et al. (2008).

Just like Fettweis et al. (2008), this study applies this SMB GrIS variability estimation to the whole 21st century by using summer temperature and annual precipitation changes (compared to 1970–1999) projected for three GHG scenarios. Nevertheless, as parameters a and b are kept constant throughout the whole period, it is assumed that the future SMB dependence on temperature and precipitation anomalies is the same as the present-day one.

The GrIS SMB anomalies for the SRES A1B scenario (a mid-range scenario) are of good quality throughout the 21st century and are calculated in average at $-300 km^3$/year for the 2090–2100 decade (Fig. 9a). For the SRES A2 scenario (i.e. with high GHG concentration), the projected SMB anomaly by the end of this century is estimated at $-350 km^3$/year by HADCM3 and HADGEM1. The MPI model projects SMB anomaly rather similar to the one projected by MPI for the SRES A1B scenario. For the SRES B1 scenario (i.e. with low GHG concentration), the projected anomaly is estimated at $-200 km^3$/year by MPI and HADCM3. The cumulated sea-level change equivalent to these anomalies should correspond to a rise of about 3.5, 5 and 6 cm by 2100 for the SRES B1, A1B and A2 scenarios, respectively (Fig. 9b). These results are in full agreement with IPCC (2007).

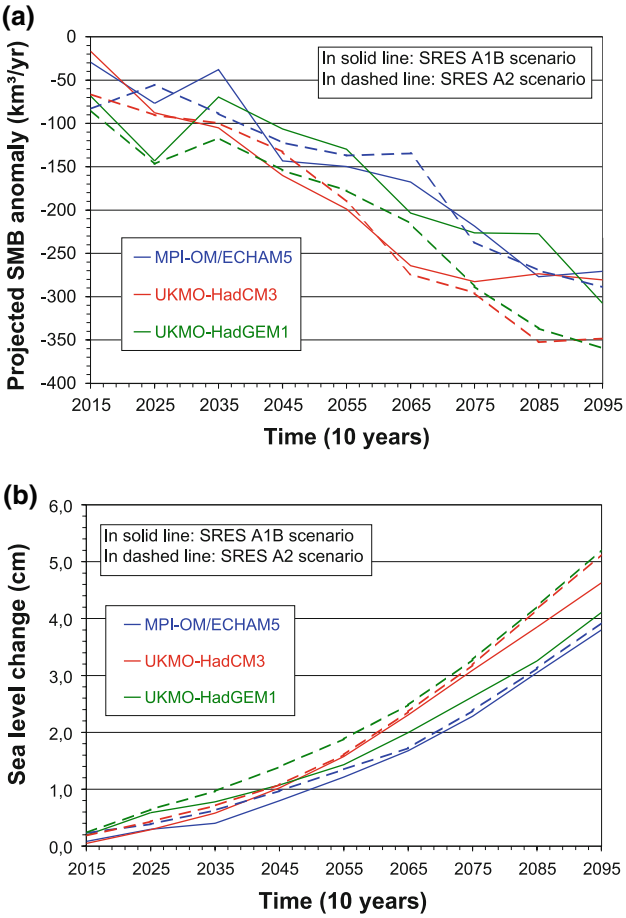

Fig. 9 **a** Time series of projected SMB anomalies for the 21st century, using AOGCMs outputs. The anomalies are decadal means and refer to the 1970–1999 period; for this period, the mean SMB rate is calculated at 350 km^3/year. **b** The same as **a**, but for the projected GrIS SMB changes expressed in equivalent sea-level rise (in cm). The computation used an ocean area of 361million km^2

The multiple regression model providing the GrIS SMB anomalies for the 21st century is only based on temperature and precipitation changes averaged over large parts of the GrIS (Fettweis et al. 2008). Nonetheless, the selected AOGCMs future projections emphazise highest increases in precipitation in the northeastern GrIS (up to +80 mmWE/year depending on the GHG emissions scenarios) (Fig. 6b), while increases in temperature are more homogeneous (Fig. 7a). However, only small changes (from −10 to +10 mmWE/year) are projected in the areas with the highest melting rates under the present-day climate (as along the western coasts). The winter accumulation not only builds up ice mass but also impacts the summer melt via the ice-albedo feedback (Mote 2003). This suggests that negative SMB anomalies higher than those approximated here are likely to occur in areas undergoing nowadays intense melting and that positive SMB anomalies (induced by higher accumulation rates)

should occur in the eastern part of the GrIS. Consequently, approximations only based on whole ice sheet modification (Gregory and Huybrechts 2006; Fettweis et al. 2008) could underestimate SMB changes over the GrIS. Therefore, only full surface–atmosphere coupled simulations should be considered as suitable for gauging future SMB changes.

Circulation anomaly patterns in 2008 were close to the ones projected for the end of the 21st century. Indeed, the 500 hPa geopotential height simulations carried out by both the reanalyses show a positive anomaly in the northern GrIS (up to +40 gpm) but no anomaly in the southwestern GrIS (see Fig. 10). This induces a zonal circulation strengthening, as projected for the future. Therefore, the 2008 atmospheric circulation could be considered as an approximation of GrIS future climate conditions. In 2008, anomalies results induced an extreme snow melt (associated to a temperature 3°C higher than normal) in the northern part of the ice sheet. This melting was associated to a weakening east-to-west circulation (Tedesco et al. 2008b; Box et al. 2009). The ERA-40 and NCEP1 simulate negative annual precipitation anomalies in the western part of Greenland (up to −40mmWE/year) and positive anomalies in the eastern part (up to + 60mmWE/year). Finally, the SMB 1971–2000 anomaly simulated for 2008 is evaluated at -150km^3/year by the Polar MM5 Model (Box et al. 2006), -50km^3/year by Hanna et al. (2008) and -200km^3/year by the MAR model (Fettweis 2007), which is in agreement with the future projections.

6 Discussion and conclusion

Results from AOGCMs for the IPCC AR4 are used to select the AOGCMs most suited to model the GrIS present-day climate (1970–1999), because future projections established by global models that are unable to reproduce the present-day climate over the GrIS accurately have little reliability. The models are evaluated on the basis of their ability to simulate atmospheric circulation (500 hPa geopotential height), the NAO (standard deviation of 500 hPa geopotential height), and the surface conditions (near-surface temperature and annual precipitation). However, no AOGCM is able to model with full reliability both the general circulation and surface conditions of the present-day climate. Consequently, we decided to model circulation and surface conditions with MPI, HADCM3 and HADGEM1 as "middle-way" models.

These three selected AOGCMs are then used to project the changes planned by three IPCC GHG emissions scenarios (B1, A1B and A2). Compared to present-day climate, the highest anomalies of the 500 hPa geopotential height are projected to take place in northern Greenland,

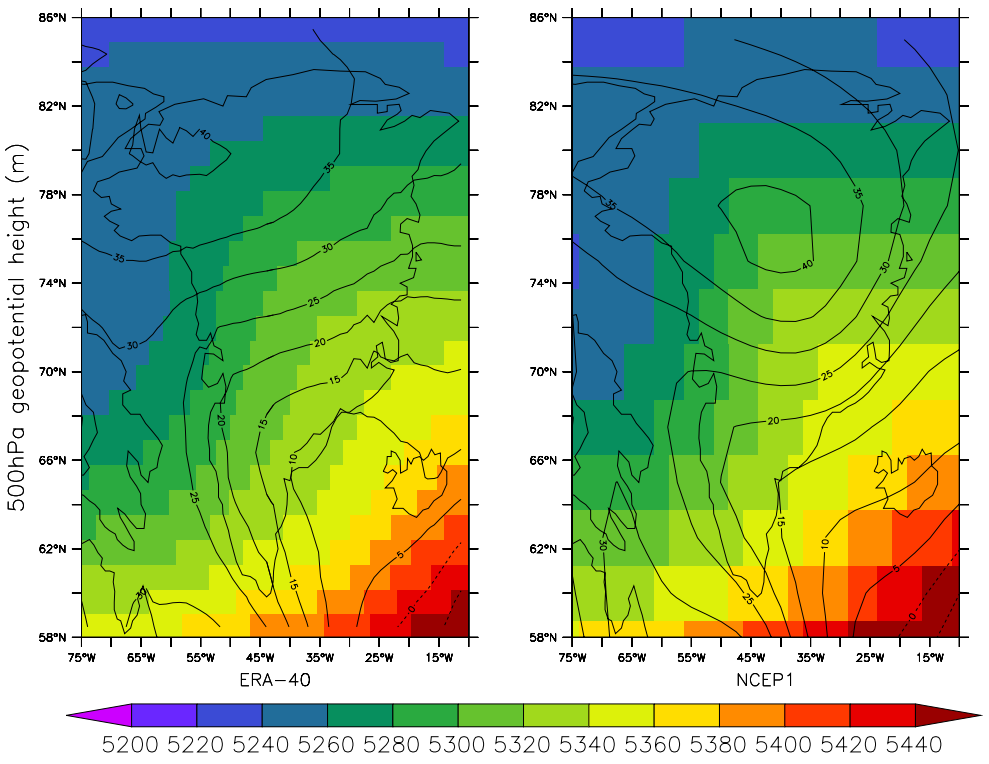

Fig. 10 Annual 500 hPa geopotential height (in gpm) simulated by the ECMWF operational analysis and the NCEP1 reanalysis for 2008. Anomalies (in gpm) referred to the 1970–1999 period. The 500 hPa geopotential height means are drawn in *solid lines* (positive anomalies) and in *dashed lines* (negative anomalies)

dampen the west-to-east circulation (zonal flow) and enhance the meridional fluxes, providing more heat and moisture to the GrIS. The atmospheric circulation changes induce higher precipitation only over the northeastern GrIS (+60 mmWE/year in 2100). The annual temperature rise should reach up to +4°C in average over the GrIS and be more pronounced along the northern coast (about +8°C) due to changes in Arctic sea ice concentration.

Finally, we provide estimations of the GrIS SMB changes from 2010 to 2100 based on a multiple regression model. The regression model uses AOGCM-projected anomalies of GrIS summer temperature and GrIS annual precipitation, computed on specific regions for the 1970–1999 period and extended into the 21st century. The projected SMB anomalies are estimated at $-300 km^3$/year in 2100 compared to the present-day climate and lead to about 5 cm of sea-level rise, as projected by IPCC (2007).

While the main purpose of this work is to find reliable AOGCMs for regional downscaling studies, we admit that our choice of investigated parameters as well as AOGCMs-selection criteria is questionable. The emphasis was mainly put on the models ability to reproduce atmospheric circulation patterns around Greenland and the NAO, through the 500 hPa geopotential height and its interannual variability, respectively. These parameters give important indications about whether an AOGCM can be used for forcing a regional model. In addition, GrIS surface parameters such as precipitation or near-surface temperature are strongly affected by large-scale atmospheric circulation and its variability.

In conformity with what Connolley and Bracegirdle (2007) and Lefebvre and Goosse (2007) found for Antartica, the AOGCMs average compares well with observations and reanalyses over Greenland. Even if it can provide more accurate results in modelling the present-day climate than any individual model, the average-based AOGCMs outputs cannot be used as regional model boundaries conditions for future projection attempts.

The skill-scores method provides us a way to differentiate between the AOGCMs (Connolley and Bracegirdle 2007), but it does not gauge the accuracy of several parameters considered in our study, such as the quality of atmospheric circulation pattern, location of precipitation minimum/maximum, and NAO modelling. However, Connolley and Bracegirdle (2007) obtained the highest skill scores with MPI and HADGEM1 when assessed against Antarctica measures as well as global measures. These are two of the three most suitable models for simulating present-day climate over Greenland that were selected in our representation–skill approach. Moreover, as deduced from Tables 1 and 2, the high resolution of some AOGCMS (e.g. INGV, MIROC-HR or CCSM3) can slightly improve their skill scores or their representation skill over Greenland, but it is no sufficient condition to model the GrIS with a satisfactory accuracy (especially the atmospheric circulation and its variability).

Our regression-based approximations could underestimate the GrIS SMB changes resulting from global warming because the regression model is only based on temperature and precipitation changes averaged over the whole GrIS. Indeed, precipitation changes projected for the 21st century are confined in northeastern part of Greenland, while temperature rises are more homogeneous over the GrIS. This suggests that negative SMB anomalies higher than those projected should occur in the areas currently characterised by intense melting. On the contrary, positive SMB anomalies (induced by higher accumulation rates) could occur in the eastern GrIS.

Therefore, full high-resolution surface–atmosphere coupled simulation could be more suitable to estimate future SMB changes, knowing that large uncertainties remain in these GrIS SMB projections based solely on global model outputs. A regional model coupled with a snow model and nested in an AOGCM is particularly well designed for this kind of study, by offering more sophisticated physics and surface parametrizations adapted for polar regions (Hanna et al. 2008 and Mernild et al. 2008). However, the mid-tropospheric atmospheric circulation is fully induced in a regional model by the AOGCM model used as forcing for its boundaries. Therefore, it is essential to have an appropriate forcing global model for general circulation modelling.

Acknowledgements Bruno Franco is a research fellow from the Belgian National Fund for Scientific Research (FNRS). We acknowledge the modelling groups, the Program for Climate Model Diagnosis and Intercomparison (PCMDI) and the WCRP's Working Group on Coupled Modelling (WGCM) for their roles in making available the WRCP CMIP3 multi-model dataset. Support of this dataset is provided by the Office of Science, US Department of Energy. We also thank the European Centre for Medium–Range Weather Forecasts (ECMWF) for ECMWF reanalysis. The NCEP/NCAR reanalysis is provided by the NOAA/OAR/ESRL PSD, Boulder, Colorado, USA, from their Web site at http://www.cdc.noaa.gov/. Finally, the authors want to thank A. Prick for her precious spell check in this manuscript.

References

Appenzeller C, Schwander J, Sommer S, Stocker TF (1998) The North Atlantic Oscillation and its imprint on precipitation and ice accumulation in Greenland. Geophys Res Lett 25(11):1939–1942

Bales RC, Guo Q, Shen D, McConnell JR, Du G, Burkhart JF, Spikes VB, Hanna E, Cappelen J (2009) Annual accumulation for Greenland updated using ice core data developed during 2000–2006 and analysis of daily coastal meteorological data. Geophys Res Lett 114:D06116. doi:10.1029/2008JD011208

Barry RG, Kiladis GN (1982) Climatic characteristics of Greenland. In: Radok U (ed) Climatic and Physical Characteristics of the Greenland ice sheet. CIRES, Boulder, CO, USA, pp 7–33

Bond G, Broecker W, Johnsen S, McManus J, Labeyrie L, Jouzel J, Bonami G (1993) Correlations between climate records from North Atlantic sediments and Greenland Ice. Nature 365:143–147

Box JE (2002) Survey of Greenland instrumental temperature records: 1873–2001. Int J Climatol 22:1829–1847

Box JE, Bromwich DH, Bai LS (2004) Greenland ice sheet surface mass balance for 1991–2000: application of Polar MM5 mesoscale model and in–situ data. J Geophys Res 109(D16):D16105. doi:10.1029/2003JD004451

Box JE, Bromwich DH, Veenhuis BA, Bai LS, Stroeve JC, Rogers JC, Steffen K, Haran T, Wang SH (2006) Greenland ice sheet surface mass balance variability (1988–2004) from calibrated Polar MM5 output. J Clim 19(12):2783–2800

Box JE, Bai LS, Benson R, Bhattacharya I, Bromwich DH, Cappelen J, Decker D, DiGirolamo N, Fettweis X, Hall D, Hanna E, Mote T, Tedesco M, van de Wal R, van den Broeke M (2009) Greenland climate in 2008. In: State of the climate in 2008. Bulletin of the American Meteorological Society, vol 90, no 8, pp S1–S196. doi:10.1175/BAMS-90-8-StateoftheClimate

Bromwich DH, Chen QS, Li YF, Cullather RI (1999) Precipitation over Greenland and its relation to the North Atlantic Oscillation. J Geophys Res 104(D18):22103–22115

Burgess EW, Forster RR, Box JE, Smith LC, Bromwich DH (2009) Greenland ice sheet annually-resolved accumulation rates (1958–2007), a spatially calibrated model. J Geophys Res (provisionally accepted)

Cappelen J, Jorgensen BV, Laursen EV, Stannius LS, Thomsen RS (2001) The observed climate of Greenland, 1958–99—with climatological standard normals, 1961–1990. Tech Rep 00–18, Danish Meteorological Institute, Copenhagen

Chen QS, Bromwich DH, Bai L (1997) Precipitation over Greenland retrieved by a dynamic method and its relation to cyclonic activity. J Clim 10:839–870

Chylek P, Box JE, Lesins G (2004) Global warming and the Greenland ice sheet. Clim Change 63:201–221

Comiso C, Parkinson CL, Gerttsen R, Stock L (2008) Accelerated decline in the Arctic sea ice cover. Geophys Res Lett 35:L01703. doi:10.1029/2007GL031972

Connolley WM, Bracegirdle TJ (2007) An Antarctic assessment of IPCC AR4 coupled models. Geophys Res Lett 34:L22505. doi:10.1029/2007GL031648

Cuffey KM, Marshall SJ (2000) Substantial contribution to sea level rise during the last interglacial from the Greenland ice sheet. Nature 404:591–594

Dethloff K, Schwager M, Christensen JH, Kiilsholm S, Rinke A, Dorn W, Jung-Rothenhusler F, Fischer H, Kipfstuhl S, Miller H (2002) Recent Greenland accumulation estimated from regional model simulations and ice core analysis. J Clim 15:2821–2832

Fettweis X, Galle H, Lefebre L, van Ypersele JP (2005) Greenland surface mass balance simulated by a regional climate model and comparison with satellite derived data in 1990–1991. Clim Dyn 24:623–640. doi:10.1007/s00382-005-0010-y

Fettweis X (2007) Reconstruction of the 1979–2006 Greenland ice sheet surface mass balance using the regional climate model MAR. The Cryosphere 1:21–40

Fettweis X, Hanna E, Galle H, Huybrechts P, Erpicum M (2008) Estimation of the Greenland ice sheet surface mass balance for the 20th and 21st centuries. The Cryosphere 2:117–129

Gallée H, Duynkerke P (1997) Air–snow interactions and the surface energy and mass balance over the melting zone of West Greenland during GIMEX. J Geophys Res 102:13813–13824

Gregory JM, Dixon K, Stouffer RJ, Weaver A, Driesschaert E, Eby M, Fichefet T, Hasumi H, Hu A, Jungclaus J, Kamenkovich I, Levermann A, Montoya M, Murakami S, Nawrath S, Oka A, Solokov A, Thorpe R (2005) A model intercomparison of changes in the Atlantic thermohaline circulation in response to increasing atmospheric concentration. J Geophys Res 32:L12703. doi:10.1029/2005GL023209

Gregory JM, Huybrechts P (2006) Ice-sheet contributions to future sea-level change. Phil Trans R Soc A 364:1709–1731. doi:10.1098/rsta.2006.1796

Hanna E, Huybrechts P, Steffen K, Cappelen J, Huff R, Shuman C, Irvine–Fynn T, Wise S, Griffiths M (2008) Increased runoff from melt from the Greenland ice sheet: a response to global warming. J Clim 21:331–341. doi:10.1175/2007JCLI1964.1

Hurrell JW (1995) Decadal trends in the North Atlantic oscillation: regional temperatures and precipitation. Science 269:676–679

IPCC (2007) In: Solomon S, Qin D, Manning M, Chen Z, Marquis M, Averyt KB, Tignor M, Miller HL (eds) Climate change 2007: the physical science basis. Contribution of Working Group I to the Fourth Assessment Report of the Intergovernmental panel on Climate change. Cambridge University Press, Cambridge, UK and New York, NY, USA

Jones PD, New M, Parker DE, Martin S, Rigor IG (1999) Surface air temperature and its changes over the past 150 years. Rev Geophys 37(2):173–199

Kapsner WR, Alley RB, Shuman CA, Anandakrishnan S, Grootes PM (1995) Dominant influence of atmospheric circulation on snow accumulation in Greenland over the last 18,000 years. Nature 373:52–54. doi:10.1038/373052a0

Kiilsholm S, Christensen JH, Dethloff K, Rinke A (2003) Net accumulation of the Greenland ice sheet: high-resolution climate modelling of regional climate change in the Arctic. Geophys Res Lett 30:1485. doi:10.1029/2002GL015742

Krinner G, Julien N (2007) High-resolution simulations of the surface mass balance of Greenland at the end of this century. The Cryosphere Discuss 1:351–383

Kristjánsson JE, McInnes H (1999) The impact of Greenland on cyclone evolution in the North Atlantic. Quart J R Meteorol Soc 125:2819–2834

Kwok R, Rothrock DA (1999) Variability of Fram Strait ice flux and North Atlantic Oscillation. J Geophys Res 104(C3):5177–5189

Lefebvre W, Goosse H (2007) Analysis of the projected regional sea–ice changes in the Southern Ocean during the twenty-first century. Clim Dyn 30:59–76. doi:10.1007/s00382-007-0273-6

Leloup J, Lengaigne M, Boulanger JP (2007) Twentieth century ENSO characteristics in the IPCC database. Clim Dyn 30:277–291. doi:10.1007/s00382-007-0284-3

Meehl GA, Stocker TF, Collins WD, Friedlingstein P, Gaye AT, Gregory JM, Kitoh A, Knutti R, Murphy JM, Noda A, Raper SCB, Watterson IG, Weaver AJ, Zhao ZC (2007) Global climate projections. In: Solomon S, Qin D, Manning M, Chen Z, Marquis M, Averyt KB, Tignor M, Miller HL (eds) Climate change 2007: the physical science basis. Contribution of Working Group I to the Fourth Assessment Report of the Intergovernmental Panel on Climate Change. Cambridge University Press, Cambridge, UK and New York, NY, USA

Mernild SH, Liston GE, Hiemstra CA, Steffen K (2008) Surface melt area and water balance modeling on the Greenland ice sheet 1995–2005. J Hydrometeorol 9(6):1191–1211

Mosley-Thompson E, Readinger CR, Craigmile P, Thompson LG, Calder CA (2005) Regional sensitivity of Greenland precipitation to NAO variability. Geophys Res Lett 32:L24707. doi:10.1029/2005GL024776

Mote TL (2003) Estimation of runoff rates, mass balance, and elevation changes on the Greenland ice sheet from passive microwave observations. J Geophys Res 108(D2):4056. doi:10.1029/2001JD002032

Ohmura A, Reeh N (1991) New precipitation and accumulation maps for Greenland. J Glaciol 37:140–148

Parkinson CL, Cavalieri DJ, Gloersen P, Zwally HJ, Comiso JC (1999) Arctic sea ice extents, areas, and trends, 1978–1996. J Geophys Res 104(C9):20837–20856

Rahmstorf S, Crucifix M, Ganopolski A, Goosse H, Kamenkovich I, Knutti R, Lohmann G, Marsh R, Mysak LA, Wang Z, Weaver AJ (2005) Thermohaline circulation hysteresis: a model intercomparison. Geophys Res Lett 32(23):L23605. doi:10.1029/2005GL023655

Rogers JC (1997) North Atlantic storm track variability and its association to the North Atlantic Oscillation and climate variability of Northern Europe. J Clim 10(7):1635–1647

Stendel M, Christensen JH, Petersen D (2008) Arctic climate and climate change with a focus on Greenland. Adv Ecol Res 40:13–43. doi:10.1016/S0065-2504(07)00002-5

Steffen K (1995) Surface energy exchange at the equilibrium line on the Greenland ice sheet during onset of melt. Ann Glaciol 21:13–18

Steffen K, Box J (2001) Surface climatology of the Greenland ice sheet: Greenland climate network 1995–1999. J Geophys Res 106(D24):33951–33964

Swingedouw D, Braconnot P, Marti O (2006) Sensitivity of the Atlantic meridional overturning circulation to the melting from northern glaciers in climate change experiments. Geophys Res Lett 33:L10503. doi:10.1029/2006GL026075

Tedesco M, Serreze M, Fettweis X (2008a) Diagnosing the extreme surface melt event over southwestern Greenland in 2007. The Cryosphere 2:159–166

Tedesco M, Fettweis X, van den Broeke MR, van de Wal RSW, Smeets CJPP (2008b) Extreme snowmelt in Northern Greenland during summer 2008. Eos Trans AGU 89(41). doi:10.1029/2008EO410004

Thompson DWJ, Wallace JM (1998) The Artic Oscillation signature in the wintertime geopotential height and temperature fields. Geophys Res Lett 9:1297–1300

Van Loon H, Rogers JC (1978) The seesaw in winter temperatures between Greenland and northern Europe: Part 1, general description. Mon Weather Rev 106(3):296–310

Walsh JE, Chapman WL, Romanovsky V, Christensen JH, Stendel M (2008) Global climate model performance over Alaska and Greenland. J Clim 21:6156–6174. doi:10.1175/2008JCLI2163.1

Wouters B, Chambers D, Schrama EJO (2008) GRACE observes small-scale mass loss in Greenland. Geophys Res Lett 35:L20501. doi:10.1029/2008GL034816

Zuo Z, Oerlemans J (1997) Contribution of glacier melt to sea-level rise since AD 1865: a regionally differentiated calculation. Clim Dyn 13(12):835–845